# Investigation of 3,4-ethylenedioxythiophene and 3,4-dimethoxythiophene as linkage units for multi-dimensional dimeric acceptors

Shaohui Yuan‡[a], Baofa Lan‡[a], Xinyi Ji[a*], Jiaying Wang[a], Wenkai Zhao[a], Guankui Long[a], Xiangjian Wan[b], Bin Kan[a*], Yongsheng Chen[b]

[a]School of Materials Science and Engineering, National Institute for Advanced Materials, Nankai University, Tianjin 300350, China.

‡ These authors contributed equally to this work.

* Corresponding E-mails: kanbin04@nankai.edu.cn; xyji06@nankai.edu.cn.

**Contents**

## 1. Materials and Synthesis.

Polymer donor PM6 and the ending unit INCN-2F were purchased from Solarmer Material (Beijing) Inc, Organtec. and Derthon, respectively. Unless otherwise specified, all the other reagents and chemicals were used directly without further purification, which purchased from commercial suppliers.

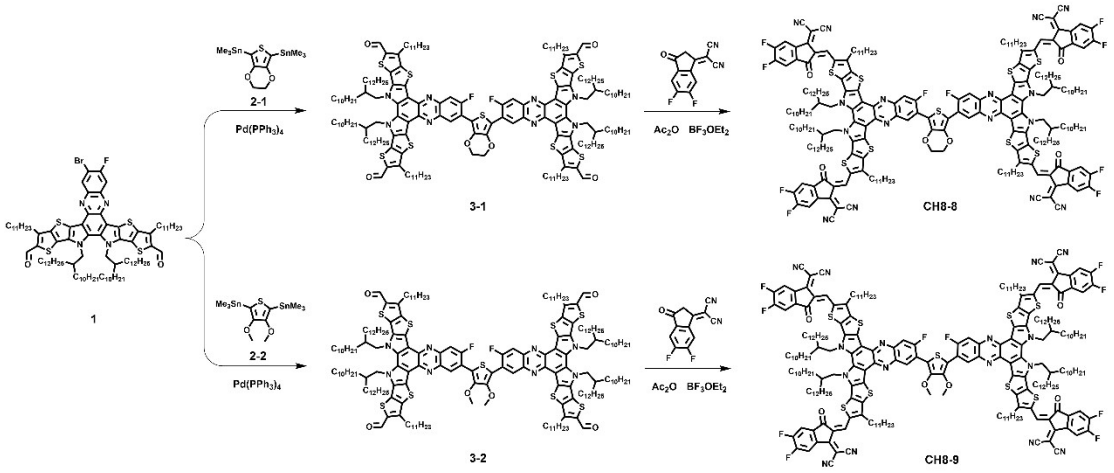


**Scheme S1.** The synthetic route to CH8-8 and CH8-9.

**Compound 1:** Compound 1 was synthesized according to previously reported method.[1]

**Compound 3-1 and 3-2:** Compound 1 (415 mg, 0.26 mmol, 1.0 eq), compound 2-1 (60 mg, 0.13 mmol, 0.5 eq) and $Pd(PPh_3)_4$ (59 mg, 0.05 mmol, 0.2 eq) were dissolved in 100 mL two-necked round bottom flask with 35 mL toluene. Then the mixture was heated to reflux for 12 h under the protection of argon. After cooling to room temperature, the reaction mixture was quenched with saturated aqueous solution of potassium fluoride for 30 min and then extracted with dichloromethane. The organic layers were combined and dried over anhydrous $Na_2SO_4$. Finally, the precipitate was purified by column chromatography on silica gel with the eluent of petroleum ether/ethyl acetate (v:v=80:1) obtained red compound 3-1 (267 mg, 65%). Compound

3-2 was synthesized by compound 1, compound 2-2 and $Pd(PPh_3)_4$ with a similar yield.

**Data for compound 3-1:** $^1$H NMR (400MHz, $CDCl_3$, ppm) δ 10.17 (s, 4H), 9.11 (d, *J* = 8 Hz, 2H), 8.17 (d, *J* = 12 Hz, 2H), 4.70-4.68 (m, 12H), 3.29-3.24 (m, 8H), 2.15-2.12 (m, 4H), 2.04-1.95 (m, 8H), 1.58 (s, 8H), 1.56-1.50 (m, 8H), 1.45-1.42 (m, 8H), 1.3-1.22 (m, 94H), 1.17-1.08 (m, 42H), 1.03-0.94 (m, 60H), 0.89-0.84 (m, 40H). $^{13}$C NMR (101MHz, $CDCl_3$, ppm) δ 181.76, 158.26, 147.01, 144.27, 141.21, 140.50, 139.14, 138.36, 136.84, 133.01, 132.76, 131.15, 129.67, 128.92, 128.22, 124.47, 118.05, 117.89, 112.87, 112.64, 112.11, 64.93, 55.42, 52.70, 38.98, 32.00, 30.48, 29.75, 29.41, 29.33, 28.31, 25.58, 22.77, 14.16. MS (m/z, MALDI): Calc. for $[C_{198}H_{300}F_2N_8O_6S_9]H^+$ 3215.16, found: 3215.60.

**Data for compound 3-2:** $^1$H NMR (400MHz, $CDCl_3$, ppm) δ 10.17 (s, 4H), 8.94 (d, *J* = 8 Hz,2H), 8.21 (d, *J* = 12 Hz), 4.70-4.68 (m, 12H), 4.09 (s, 6H), 3.28-3.24 (m, 8H), 2.16-2.11 (m, 4H), 2.03-1.95 (m, 8H), 1.57-1.52 (m, 12H), 1.43-1.40 (m, 8H), 1.33-1.22 (m, 82H), 1.14-1.10 (m, 42H), 1.03-0.94 (m, 70H), 0.89-0.82 (m, 46H). $^{13}$C NMR (101MHz, $CDCl_3$, ppm) δ 181.57, 160.86, 158.32, 148.85, 146.77, 144.36, 141.73, 141.59, 138.93, 138.64, 138.37, 136.93, 136.81, 133.13, 132.66, 129.53, 128.25, 124.66, 124.47, 118.67, 118.10, 117.82, 60.72, 55.51, 39.03, 32.00, 31.94, 30.68, 30.63, 30.56, 29.78, 29.75, 29.59, 29.56, 29.42, 29.33, 25.68, 22.75, 14.11. MS (m/z, MALDI-TOF): Calc. for $[C_{198}H_{302}F_2N_8O_6S_9]H^+$ 3217.18, found: 3217.87.

**Compound CH8-8 and CH8-9:** Compound 3-1 (200 mg, 0.06 mmol, 1 eq), 2-(5,6-difluoro-3-oxo-2,3-dihydro-1H-inden-1-ylidene) malononitrile (INCN-2F, 171 mg, 0.75 mmol, 12 eq) and $Ac_2O$ (0.15 mL), $BF_3OEt_2$ (0.15 mL) were mixed in 100 mL

single-necked round bottom flask with 15 mL toluene. Then the mixture was reacted 20 min at room temperature under the protection of argon. The reaction mixture was precipitated in 30 mL methanol. Finally, the precipitate was purified by column chromatography on silica gel with the eluent of petroleum ether/ chloroform (v:v=2:1) obtained blue CH8-8 (187 mg, 74%). CH8-9 was synthesized by compound 3-2, INCN-2F, $Ac_2O$ and $BF_3OEt_2$ with a similar yield.

**Data for CH8-8:** MS (m/z, MALDI): Calc. for $[C_{246}H_{308}F_{10}N_{16}O_6S_9]H^+$ 4063.80, found: 4064.75.

**Data for CH8-9:** MS (m/z, MALDI): Calc. for $[C_{246}H_{310}F_{10}N_{16}O_6S_9]H^+$ 4065.82, found: 4066.64.

## 2. Measurements and Instruments.

**Computational methods in this work.** All alkyl chains were replaced with methyl groups (-$CH_3$) to reduce the computational requirements. The structures were subsequently optimized with Density Functional Theory (DFT) in vacuum within the Gaussian 16 software[2]. To enhance the accuracy of the data, the structure optimization, frequency analysis and energy level of frontier molecular orbital were obtained at the Becke three-parameter Lee-Yang-Parr (B3LYP) hybrid functional[3] and lanl08(d)[4]/6-311G(d,p)[5] basis set.

**The nuclear magnetic resonance (NMR) spectra and Mass Spectra (MS).** The $^1H/^{13}C$ nuclear magnetic resonance ($^1H/^{13}C$ NMR) spectra of compounds were afforded by a Bruker AV400 Spectrometer. Time of flight mass spectrometer (TOF-MS) was obtained from Bruker Daltonics (AutoflexIII LRF200-CID).

**UV-visible (UV-vis) absorption.** UV-vis absorption spectra were obtained from a Cary 5000 UV-vis spectrophotometer.

**Electrochemical characterizations.** The cyclic voltammetry (CV) was performed on a LK98B II Microcomputer-based Electrochemical Analyzer using a glassy carbon electrode as the working electrode, a saturated calomel electrode (SCE) as reference electrode, and a Pt wire as the counter electrode. The neat CH8-8 and CH8-9 films on working electrode was in an acetonitrile solution of 0.1 mol $L^{-1}$ n-$Bu_4NPF_6$ at a scan rate of 100 mV $s^{-1}$. The ferrocene/ferrocenium was employed as internal reference. The HOMO and LUMO levels were calculated using the following equations: $E_{HOMO}$=-($E_{ox}$+4.8-$E_{Fc/Fc^+}$) eV, $E_{LUMO}$=-($E_{red}$+4.8-$E_{Fc/Fc^+}$) eV.

**Atomic force microscopy (AFM).** The AFM images were performed using in tapping mode on a Bruker Dimension Icon atomic force microscope.

**Grazing incidence wide angle X-ray scattering (GIWAXS).** The GIWAXS samples were deposited on Si substrates by the same preparation conditions with devices. The GIWAXS data were obtained at 1W1A Diffuse X-ray Scattering Station, Beijing Synchrotron Radiation Facility (BSRF-1W1A).

**$EQE_{EL}$.** For the $EQE_{EL}$ measurements, a digital source meter (Keithley 2400) was employed to inject electric current into the solar cells, and the emitted photons were collected by a Si diode (Hamamatsu s1337-1010BQ) and indicated by a picoammeter (Keithley 6482).

**Space-charge-limited current (SCLC) measurement.** The SCLC method was used to measure the hole and electron mobilities, by using a diode configuration of ITO /PEDOT:PSS/active layer/$MoO_3$/Ag for hole-only device and ITO/ZnO/active layer/ PNDIT-F3N/Ag for electron-only device. In our case, we applied forward scans for all the SCLC measurements, and hence the ITO and Al electrodes should be the anode and cathode, respectively. The dark current density curves were recorded with a bias voltage in the range of 0-8 V. The mobilities were estimated by taking current-voltage curves and fitting the results based on the equation listed below:

$$J = \frac{9\varepsilon_0\varepsilon_\gamma\mu V^2}{8L^3}$$

where $J$ is the current density, is the vacuum permittivity, $\varepsilon r$ is the relative $\varepsilon_0$ dielectric constant, $\mu$ is the mobility, and $L$ is the film thickness. $V$ ($=V_{app} - V_{bi}$) is the internal voltage in the device, where $V_{app}$ is the applied voltage to the device and $V_{bi}$ is the built-

in voltage due to the relative work function difference of the two electrodes.

**Device fabrication and measurement.** The conventional devices were fabricated with an architecture of ITO/PEDOT:PSS/PM6: Acceptors/PNDIT-F3N/Ag. In detail, the ITO glass was pre-cleaned in turn in an ultrasonic bath of detergent, deionized water, acetone and isopropanol. Then the surface of ITO was treated by UV light in an ultraviolet-ozone chamber for 15 min. A thin layer of poly(3,4-ethylene dioxythiophene):poly(styrene sulfonate) (PEDOT:PSS, Baytron PVP Al 4083) was prepared by spin-coating the PEDOT:PSS solution at 4400 rpm for 20 s on the ITO substrate. Note that the PEDOT:PSS solution was pre-filtered through a 0.45 um poly(tetrafluoroethylene) (PTFE) filter. Subsequently, the PEDOT:PSS films were baked at 160 ℃ for 15 min in air and transferred to a glove box filled with nitrogen. The PM6:CH8-8 (D/A 1:1.2) with 0.3% 1-chloronaphthalene and PM6:CH8-9 (D/A 1:1) with 0.3% 1-chloronaphthalene mixtures were fully dissolved in chloroform (CF) at a concentration of 6 mg/mL of PM6, and the resulting solutions were spin casted at 2000/1900 rpm for 30 s onto the PEDOT:PSS layer. Then the films were treated with the thermal annealing at 100˚C. The thickness of all active layers was controlled to be ~100 nm. After that, a thin layer of PNDIT-F3N (dissolved in methanol with the concentration of 1 mg/mL) was spin-coated on the top of the active layer. Finally, a layer of Ag with thickness of 150 nm was deposited under $2\times10^{-6}$ Pa. The active area of the device was 2.56 $mm^2$. The current density-voltage (J-V) curves of photovoltaic devices were recorded by a Keithley 2400 source-measure unit. The photocurrent was measured under the simulated illumination of 100 mW $cm^{-2}$ with AM1.5 G using a Enli

SS-F5-3A solar simulator, which was calibrated by a standard Si solar cell (made by Enli Technology Co., Ltd., Taiwan, and calibrated report can be traced to NREL). The thickness of the active layers was measured by a Veeco Dektak 150 profilometer. The EQE spectra were measured by using a QE-R Solar Cell. Response Measurement System (Enli Technology Co., Ltd., Taiwan).

**Energy loss analysis.** $E_{loss}$ can be calculated by the equation:

$$E_{loss} = E_g - qV_{oc}$$

Where $E_g$ is determined based on the derivatives of the EQE spectra.

The detailed components of $E_{loss}$ can be categorized into three parts based on the Shockley-Queisser (SQ) limit.

$$E_{loss} = (E_g - qV_{oc}^{SQ}) + (qV_{oc}^{SQ} - qV_{oc}^{rad}) + (qV_{oc}^{rad} - qV_{oc})$$

Where

$$V_{oc}^{SQ} = \frac{kT}{q}\ln\left(\frac{J_{sc}^{SQ}}{J_0^{SQ}} + 1\right) \cong \frac{kT}{q}\ln\left(\frac{q \cdot \int_{E_g}^{+\infty} \emptyset_{AM1.5G}(E)dE}{q \cdot \int_{E_g}^{+\infty} \emptyset_{BB}(E)dE}\right)$$

Where $\emptyset_{BB}(E)$ is black body emission at room temperature. Thus, for the unavoidable radiative recombination $\Delta E_1$:

$$\Delta E_1 = E_g - qV_{oc}^{SQ}$$

$$V_{oc}^{rad} = \frac{kT}{q}\ln\left(\frac{J_{sc}}{J_0^{rad}} + 1\right) \cong \frac{kT}{q}\ln\left(\frac{q \cdot \int_0^{+\infty} EQE(E)\emptyset_{AM1.5G}(E)dE}{q \cdot \int_0^{+\infty} EQE(E)\emptyset_{BB}(E)dE}\right)$$

Thus, for the radiative recombination $\Delta E_2$

$$\Delta E_2 = qV_{oc}^{SQ} - qV_{oc}^{rad}$$

Finally, for the non-radiative recombination loss $\Delta E_3$

$$\Delta E_3 = qV_{oc}^{rad} - qV_{oc}$$

Where $V_{OC}$ is the open circuit voltage of the OSC.

## 3. Additional Figures and Tables.

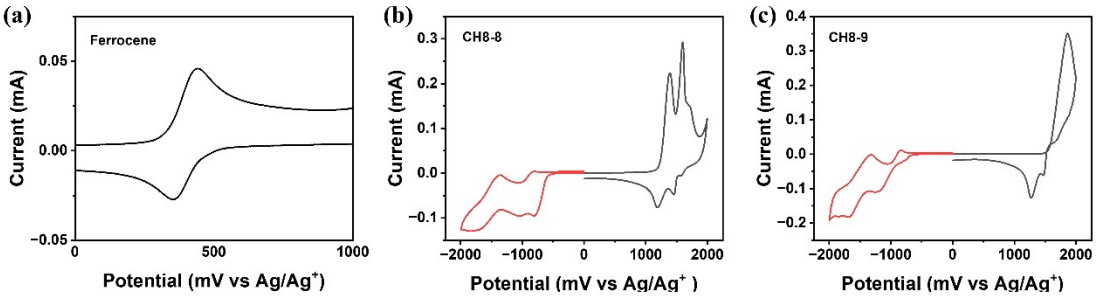


**Figure S1**. Cyclic voltammograms of (a) the reference (ferrocene) and (b) CH8-8, (c) CH8-9. The oxidation and reduction cycle was measured by films deposited on the surface of working electrode.

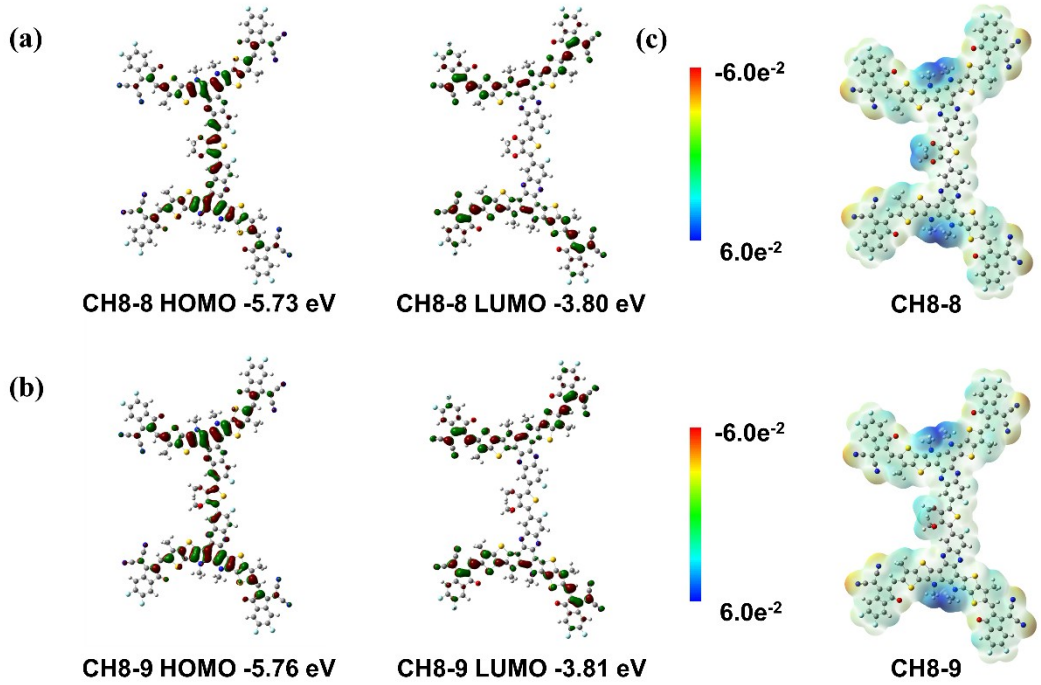


**Figure S2**. Theoretical density distribution for the frontier molecular orbits of (a) CH8-8 and (b) CH8-9, respectively. (c) ESP diagrams of CH8-8 and CH8-9.

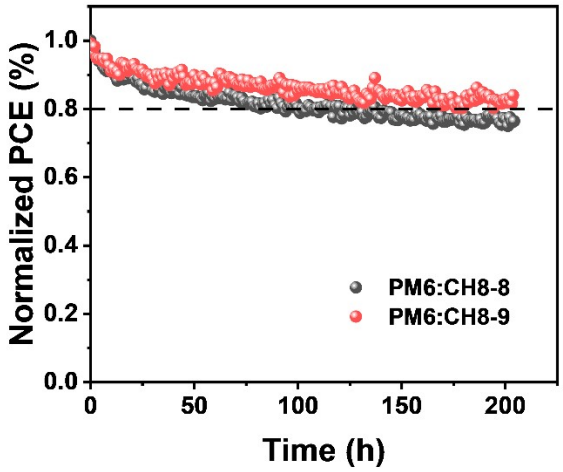


**Figure S3**. The photo-stability of PM6:CH8-8 and PM6:CH8-9 based devices.

**Table S1**. Detailed photovoltaic parameters of the PM6:CH8-8 and PM6:CH8-9 based devices processed by varied conditions under illumination of AM 1.5 G, 100 mW/cm$^2$.

| BHJ | D:A (w:w) | 1-CN (v/v) | TA (°C) | $V_{oc}$ (V) | FF (%) | $J_{sc}$ (mA cm$^{-2}$) | PCE (%) |
|---|---|---|---|---|---|---|---|
| PM6:CH8-8 | 1:0.8 | - | - | 0.931 | 55.8 | 16.44 | 8.5 |
| | 1:1.0 | | | 0.934 | 56.5 | 17.34 | 9.2 |
| | 1:1.2 | | | 0.939 | 65.3 | 19.03 | 11.7 |
| | 1:1.4 | | | 0.937 | 66.5 | 18.59 | 11.6 |
| | 1:1.2 | 0.3% | 100 | 0.932 | 70.7 | 23.92 | 15.8 |
| | | 0.5% | | 0.925 | 70.8 | 22.52 | 14.7 |
| PM6:CH8-9 | 1:0.8 | - | - | 0.940 | 65.8 | 20.53 | 12.7 |
| | 1:1.0 | | | 0.937 | 66.3 | 21.41 | 13.3 |
| | 1:1.2 | | | 0.933 | 65.7 | 21.35 | 13.1 |
| | 1:1.4 | | | 0.933 | 64.5 | 21.32 | 12.8 |
| | 1:1.0 | 0.2% | 100 | 0.924 | 71.0 | 22.87 | 15.0 |
| | | 0.3% | | 0.924 | 72.0 | 24.46 | 16.3 |
| | | 0.4% | | 0.920 | 72.3 | 23.17 | 15.4 |
| | | 0.5% | | 0.918 | 71.9 | 22.95 | 15.1 |

**Table S2**. Detailed photovoltaic parameters of the PM6:CH8-8 based devices by optimal conditions under illumination of AM 1.5 G, 100 mW/cm$^2$.

| Active layer | $V_{oc}$ (V) | FF (%) | $J_{sc}$ (mA cm$^{-2}$) | PCE (%) |
|---|---|---|---|---|
| PM6:CH8-8 | 0.931 | 69.9 | 24.04 | 15.6 |
| | 0.929 | 69.6 | 23.69 | 15.3 |
| | 0.932 | 70.7 | 23.92 | 15.8 |
| | 0.930 | 70.1 | 23.89 | 15.6 |
| | 0.928 | 70.8 | 23.91 | 15.7 |
| | 0.930 | 69.7 | 23.55 | 15.3 |
| | 0.927 | 69.5 | 24.19 | 15.6 |
| | 0.929 | 70.3 | 24.04 | 15.7 |
| | 0.929 | 70.2 | 23.35 | 15.2 |
| | 0.928 | 70.6 | 23.93 | 15.7 |
| | 0.926 | 70.3 | 24.03 | 15.6 |
| | 0.933 | 70.2 | 23.89 | 15.6 |
| | 0.932 | 69.9 | 23.97 | 15.6 |
| | 0.928 | 69.5 | 24.17 | 15.6 |
| | 0.929 | 69.2 | 24.29 | 15.6 |
| Average | 0.929 | 70.0 | 23.92 | 15.6 |

**Table S3**. Detailed photovoltaic parameters of the PM6:CH8-9 based devices by optimal conditions under illumination of AM 1.5 G, 100 mW/cm$^2$.

| Active layer | $V_{oc}$ (V) | FF (%) | $J_{sc}$ (mA cm$^{-2}$) | PCE (%) |
|---|---|---|---|---|
| PM6:CH8-9 | 0.926 | 71.8 | 24.42 | 16.2 |
| | 0.923 | 72.2 | 24.24 | 16.2 |
| | 0.922 | 72.6 | 23.88 | 16.0 |
| | 0.924 | 72.6 | 23.58 | 15.8 |
| | 0.922 | 72.5 | 23.88 | 16.0 |
| | 0.918 | 71.7 | 24.38 | 16.0 |
| | 0.919 | 71.9 | 24.26 | 16.0 |
| | 0.923 | 72.3 | 24.00 | 16.0 |
| | 0.924 | 71.8 | 24.13 | 16.0 |
| | 0.923 | 71.5 | 24.20 | 16.0 |
| | 0.925 | 71.8 | 24.05 | 16.0 |
| | 0.919 | 72.0 | 24.17 | 16.0 |
| | 0.918 | 70.6 | 24.62 | 16.0 |
| | 0.920 | 70.6 | 24.36 | 15.8 |
| | 0.924 | 72.0 | 24.46 | 16.3 |
| Average | 0.922 | 71.9 | 24.18 | 16.0 |

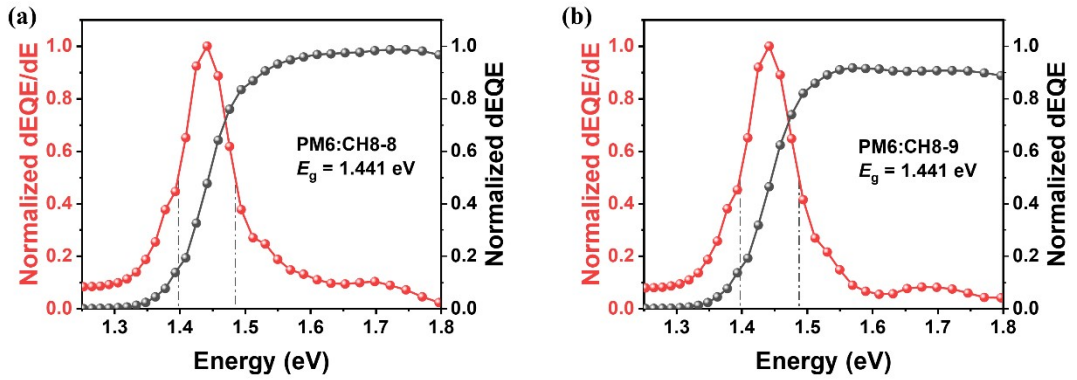


**Figure S4**. Optical bandgap determination of (a) PM6:CH8-8 and (b) PM6:CH8-9 based on the derivatives of the EQE spectra.

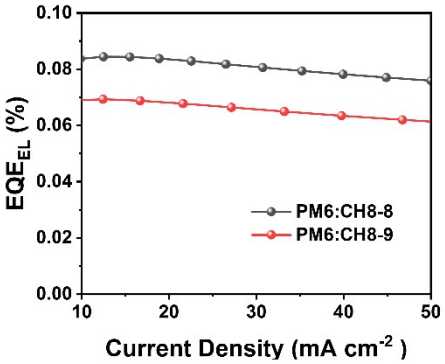


**Figure S5**. $EQE_{EL}$ spectra of PM6:CH8-8 and PM6:CH8-9 based devices.

**Table S4**. Total energy loss values and different contributions in solar cells based on the SQ limit theory.

| Active layer | $V_{oc}$ (V) | $E_g$ (eV) | $V_{oc}^{rad}$ (V) | $V_{oc}^{SQ}$ (V) | $\Delta E_1$ (eV) | $\Delta E_2$ (eV) | $\Delta E_3$ (eV) | $E_{loss}$ (eV) |
|---|---|---|---|---|---|---|---|---|
| PM6:CH8-8 | 0.928 | 1.441 | 1.087 | 1.174 | 0.267 | 0.088 | 0.183 | 0.513 |
| PM6:CH8-9 | 0.921 | 1.441 | 1.112 | 1.174 | 0.267 | 0.062 | 0.188 | 0.520 |

**Table S5.** Summary of representative part of high-performance dimeric acceptors based organic solar cells.

| Active layer | $V_{oc}$ (V) | FF (%) | $J_{sc}$ (mA cm$^{-2}$) | PCE (%) | $E_{loss}$ (eV) | Ref. |
|---|---|---|---|---|---|---|
| PM6:CH8-8 | 0.93 | 70.7 | 23.9 | 15.8 | **0.513** | ***This work*** |
| PM6:CH8-9 | 0.92 | 72.0 | 24.5 | 16.3 | **0.520** | ***This work*** |
| PM6:*d*T9TBO | 0.99 | 62.1 | 9.5 | 5.8 | **0.483** | *Angew. Chem. Int. Ed.* **2023**, 62, e202303066 |
| PM6:T0 | 0.92 | 77.1 | 24.1 | 17.1 | **0.586** | *Adv. Mater.* **2024**, 36, 2403890 |
| PM6:T1 | 0.96 | 71.7 | 21.2 | 14.6 | **0.571** | |
| PM6:T4 | 0.96 | 76.6 | 22.5 | 16.6 | **0.560** | |
| PM6:T6 | 0.97 | 76.8 | 22.9 | 17.1 | **0.553** | |
| PM6:T12 | 0.98 | 70.9 | 21.3 | 14.8 | **0.537** | |
| D18:DYF-V | 0.93 | 67.0 | 16.0 | 10.0 | **0.540** | *Adv. Funct. Mater.* **2024**, 34, 2406501 |
| D18:DYF-E | 0.94 | 75.0 | 24.2 | 17.0 | **0.530** | |
| PBQx-H-TF/dBTIC-$\delta$V-BO | 0.96 | 66.1 | 20.7 | 13.2 | **0.578** | *Adv. Funct. Mater.* **2024**, 34, 2305608 |
| PBQx-H-TF/dBTIC-$\gamma$V-BO | 0.91 | 76.6 | 24.5 | 17.1 | **0.557** | |
| PM6:CH8-0 | 0.94 | 72.1 | 22.6 | 15.3 | **0.490** | *Energy Environ. Sci.,* **2023**,16, 1773-1782 |
| PM6:CH8-1 | 0.92 | 74.2 | 24.9 | 17.1 | **0.518** | |
| PM6:CH8-2 | 0.93 | 74.9 | 24.2 | 16.8 | **0.529** | |
| PM6:CH8-3 | 0.92 | 77.0 | 24.4 | 17.2 | **0.529** | *Angew. Chem. Int. Ed.,* **2023**, e202307962 |
| PM6:CH8-4 | 0.89 | 75.5 | 26.1 | 17.6 | **0.518** | |
| PM6:CH8-5 | 0.90 | 75.2 | 24.8 | 16.8 | **0.520** | |
| PM6:DYBO | 0.97 | 75.8 | 24.6 | 18.1 | **0.484** | *Joule.,* **2023**, 7, |

| | | | | | | |
|---|---|---|---|---|---|---|
| | | | | | | 416. |
| PM6:2-BTP-2F-T | 0.91 | 78.3 | 25.5 | 18.2 | **0.531** | *Adv. Sci.*, **2022**, 9, 2202513. |
| D18:DY-T | 0.95 | 72.5 | 22.6 | 15.5 | **0.499** | *CCS Chem.*, **2023**, 5, 2576 |
| D18:DY-TF | 0.95 | 72.9 | 24.4 | 16.8 | **0.495** | |
| D18:DYF-TF | 0.94 | 75.3 | 25.8 | 18.3 | **0.493** | |
| PM6:DYSe-1 | 0.89 | 76.6 | 27.5 | 18.6 | **0.520** | *Adv. Energy Mater.* **2024**, 14, 2400938 |
| PM6:DYSe-2 | 0.88 | 75.2 | 27.5 | 18.2 | **0.522** | |

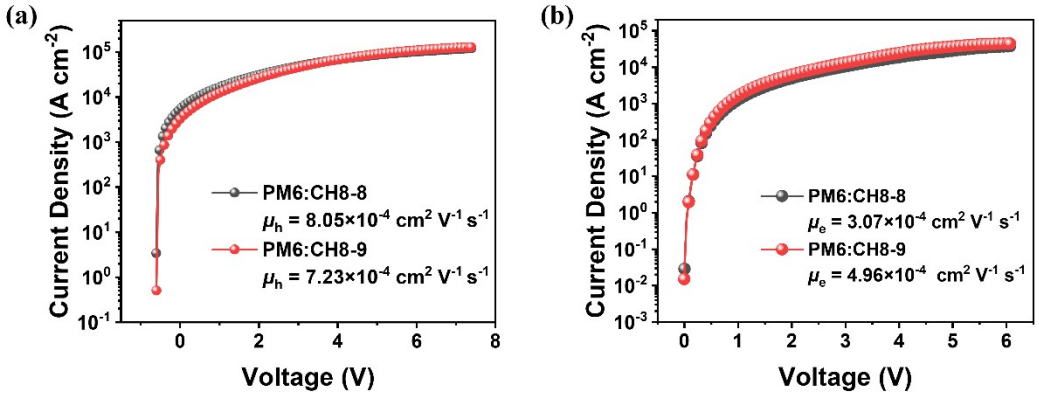


**Figure S6**. (a) Hole and (b) electron curves of PM6:CH8-8, PM6:CH8-9 based optimal devices, respectively.

**Table S6**. Charge carrier transport parameters of the optimized BHJ blends and devices.

| Active layer | $\mu_h$ ($\times10^{-4}$ cm$^{-2}$ V$^{-1}$ s$^{-1}$) | $\mu_e$ ($\times10^{-4}$ cm$^{-2}$ V$^{-1}$ s$^{-1}$) | $\mu_h/\mu_e$ |
|---|---|---|---|
| PM6:CH8-8 | 8.05 | 3.07 | 2.62 |
| PM6:CH8-9 | 7.23 | 4.96 | 1.46 |

**Table S7**. Summary of the GIWAXS parameters for the neat acceptor films and blend films.

| Film | (100) | | | (010) | | |
|---|---|---|---|---|---|---|
| | q (Å$^{-1}$) | d$^{a}$ (Å) | CL$^{b}$ (Å) | q (Å$^{-1}$) | d$^{a}$ (Å) | CL$^{b}$ (Å) |
| **CH8-8** | 0.267 | 22.53 | 38.25 | 1.604 | 3.92 | 15.54 |
| **CH8-9** | 0.270 | 23.30 | 37.74 | 1.606 | 3.91 | 22.40 |
| **PM6: CH8-8** | 0.275 | 22.86 | 57.70 | 1.626 | 3.87 | 12.20 |
| **PM6:CH8-9** | 0.274 | 22.93 | 61.11 | 1.637 | 3.84 | 14.20 |

a) Calculated from the equation: d-spacing = 2π/q.

b) Obtained from the Scherrer equation: CL = 2πK/FWHM, where FWHM is the full-width at half-maximum and K is a shape factor (K = 0.9 here).

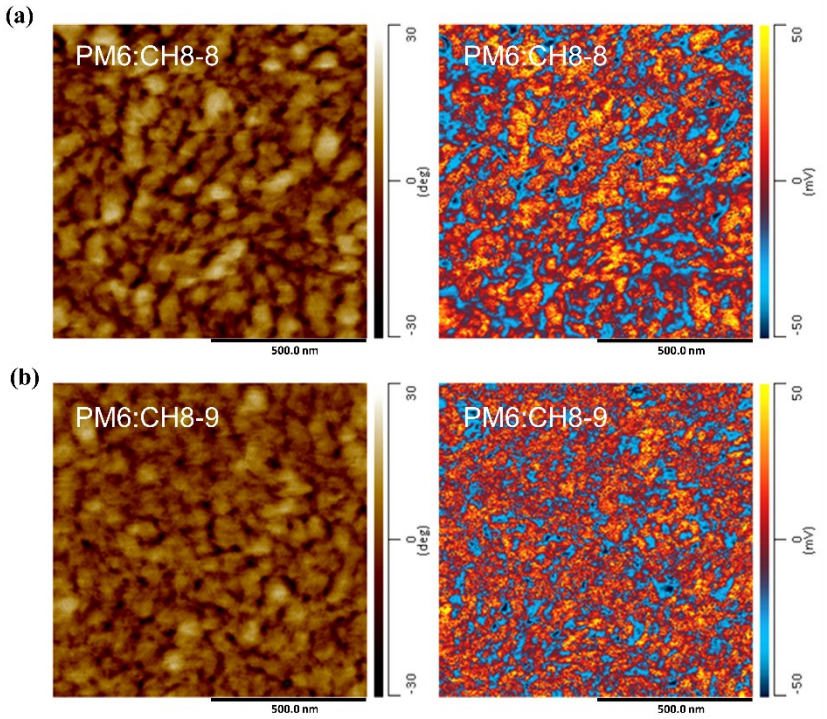


**Figure S7**. The IR-AFM image of PM6: Acceptor blend films.

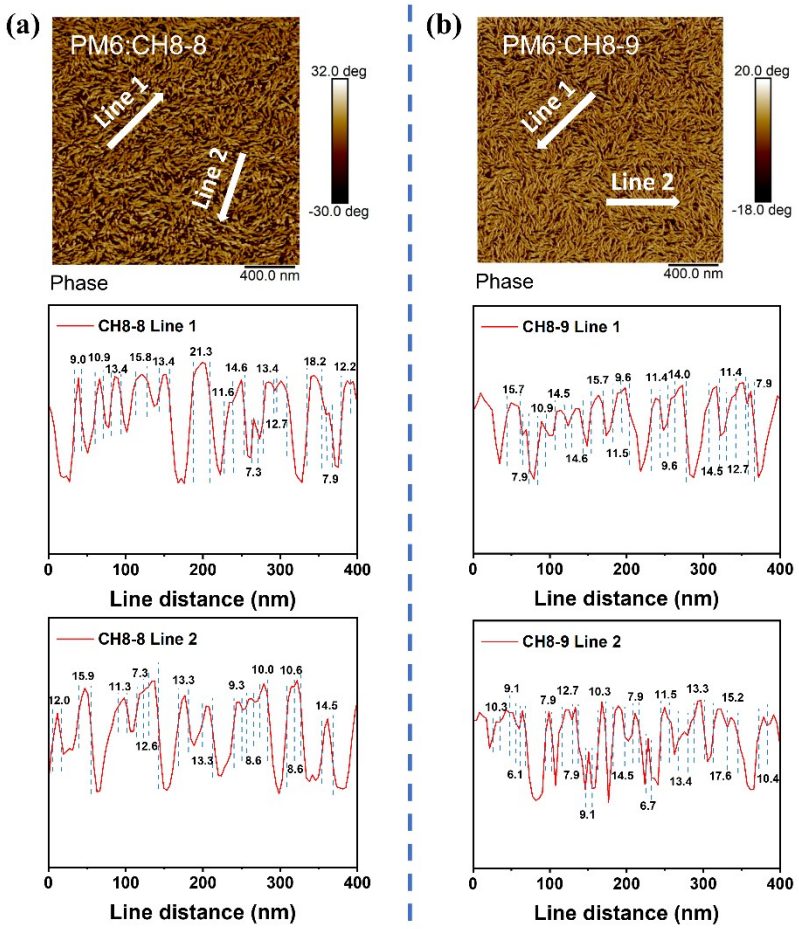


**Figure S8**. The line profile to obtain the fibril width for the (a) PM6:CH8-8, (b) PM6:CH8-9 blend films.

## 4. Spectral Charts of NMR and MS.

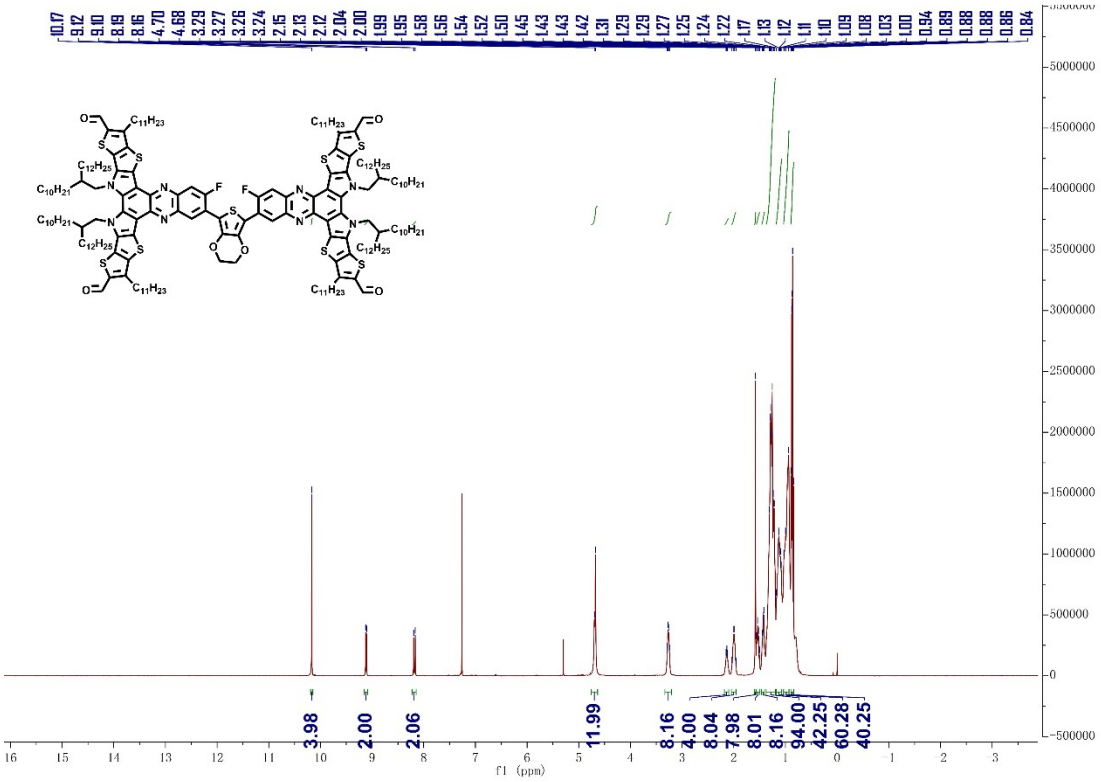

**Figure S9**. $^{1}$H NMR spectrum of compound 3-1 at 300K in $CDCl_3$.

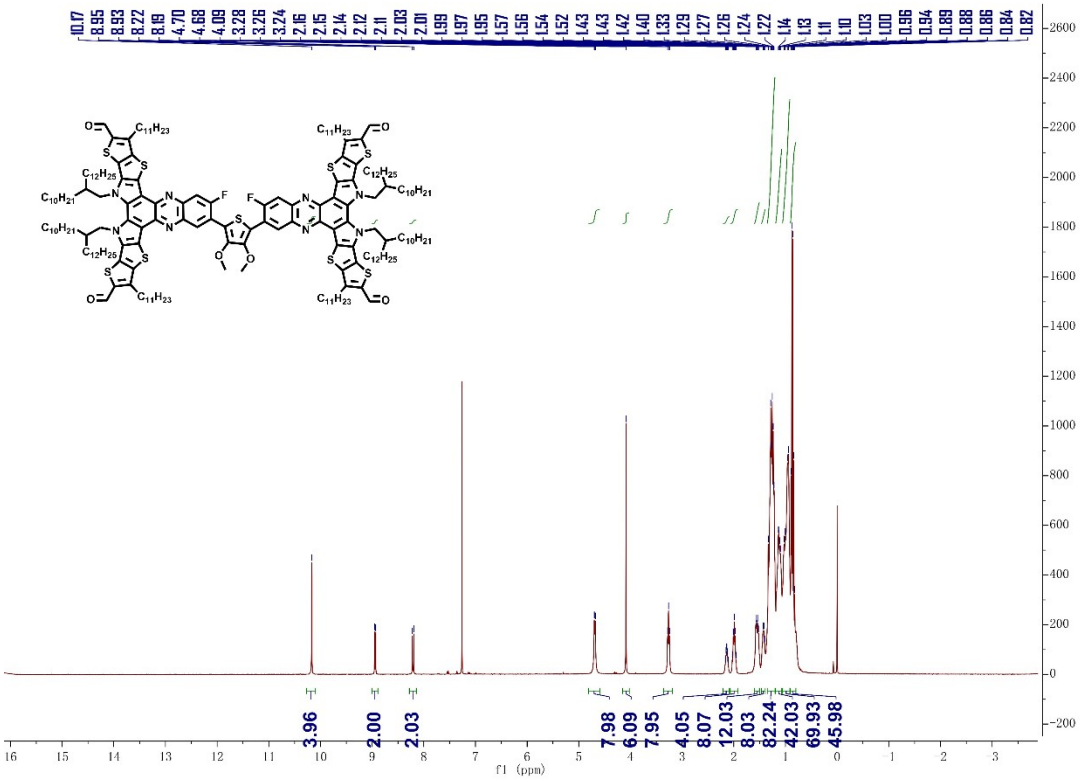

**Figure S10**. $^{1}$H NMR spectrum of compound 3-2 at 300K in $CDCl_3$.

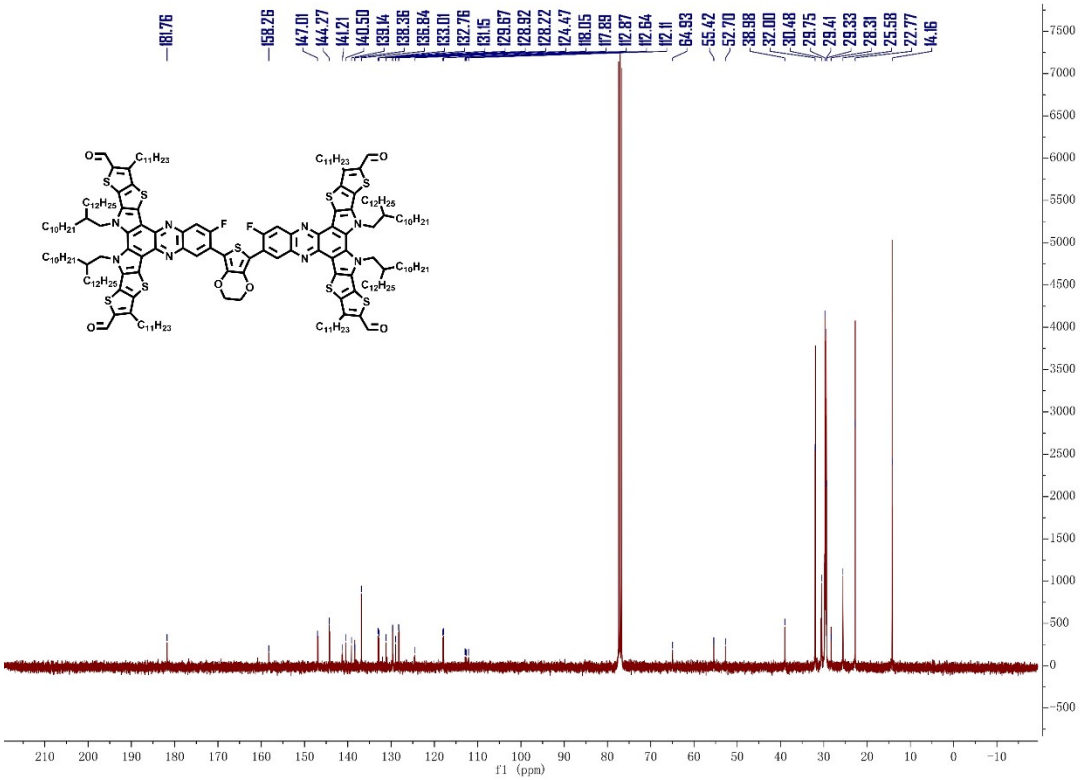

**Figure S11**. $^{13}C$ NMR spectrum of compound 3-1 at 300K in $CDCl_3$.

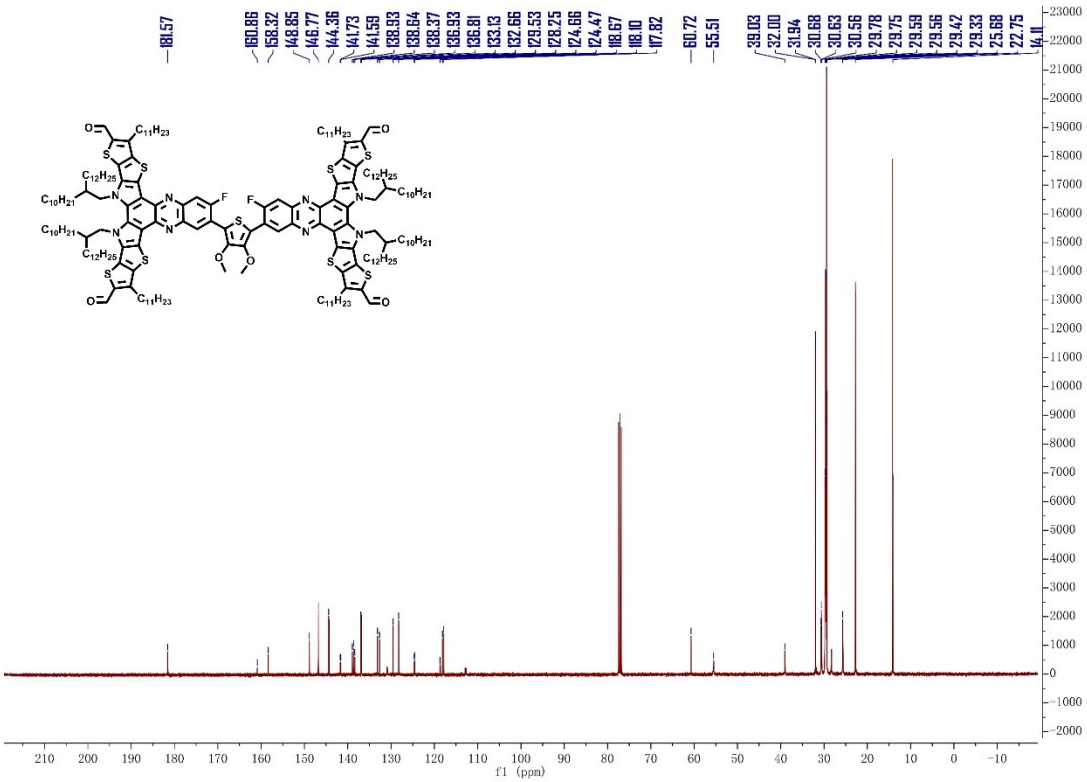

**Figure S12.** $^{13}C$ NMR spectrum of compound 3-2 at 300K in $CDCl_3$.

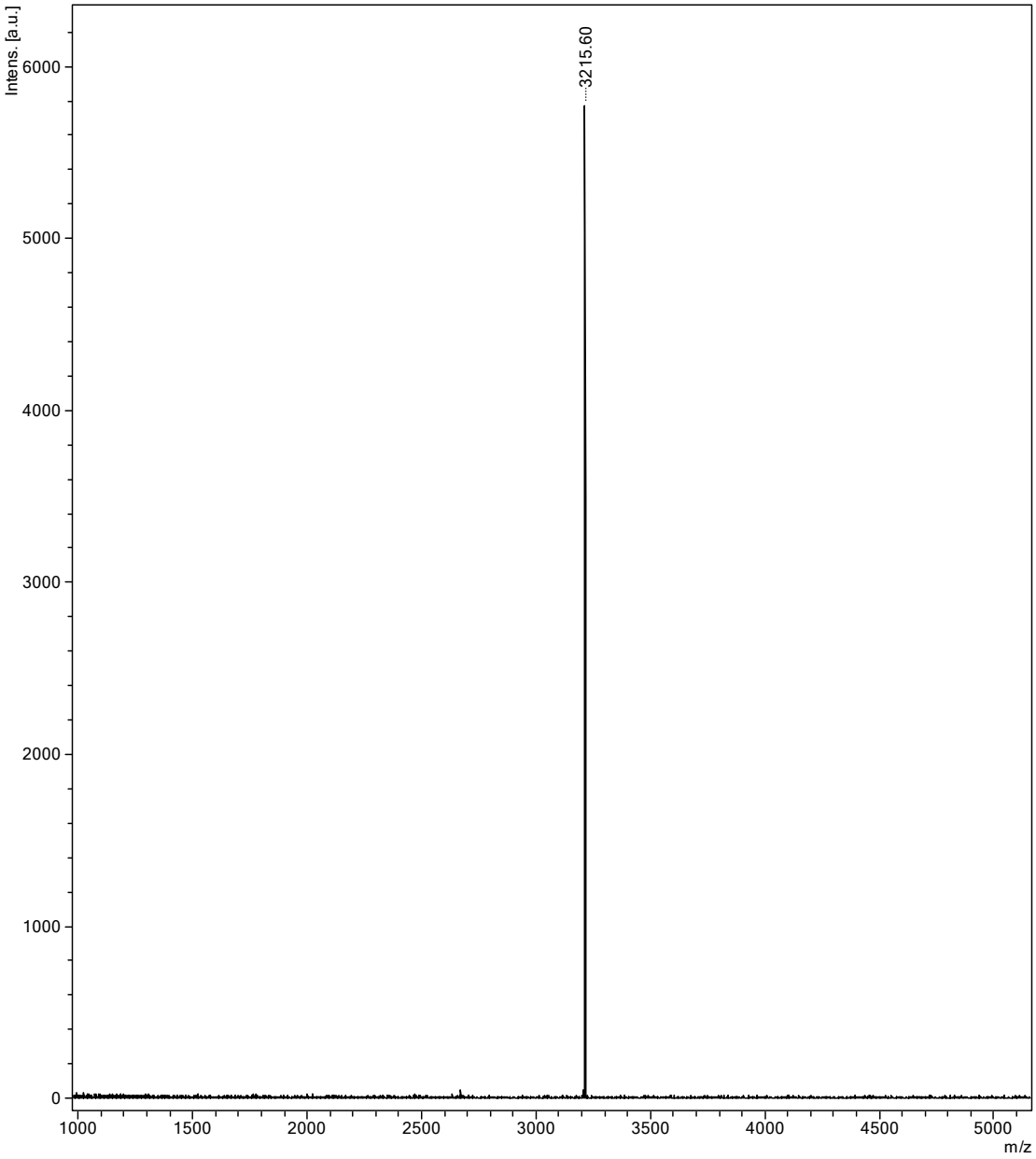


**Figure S13.** MS of compound 3-1.

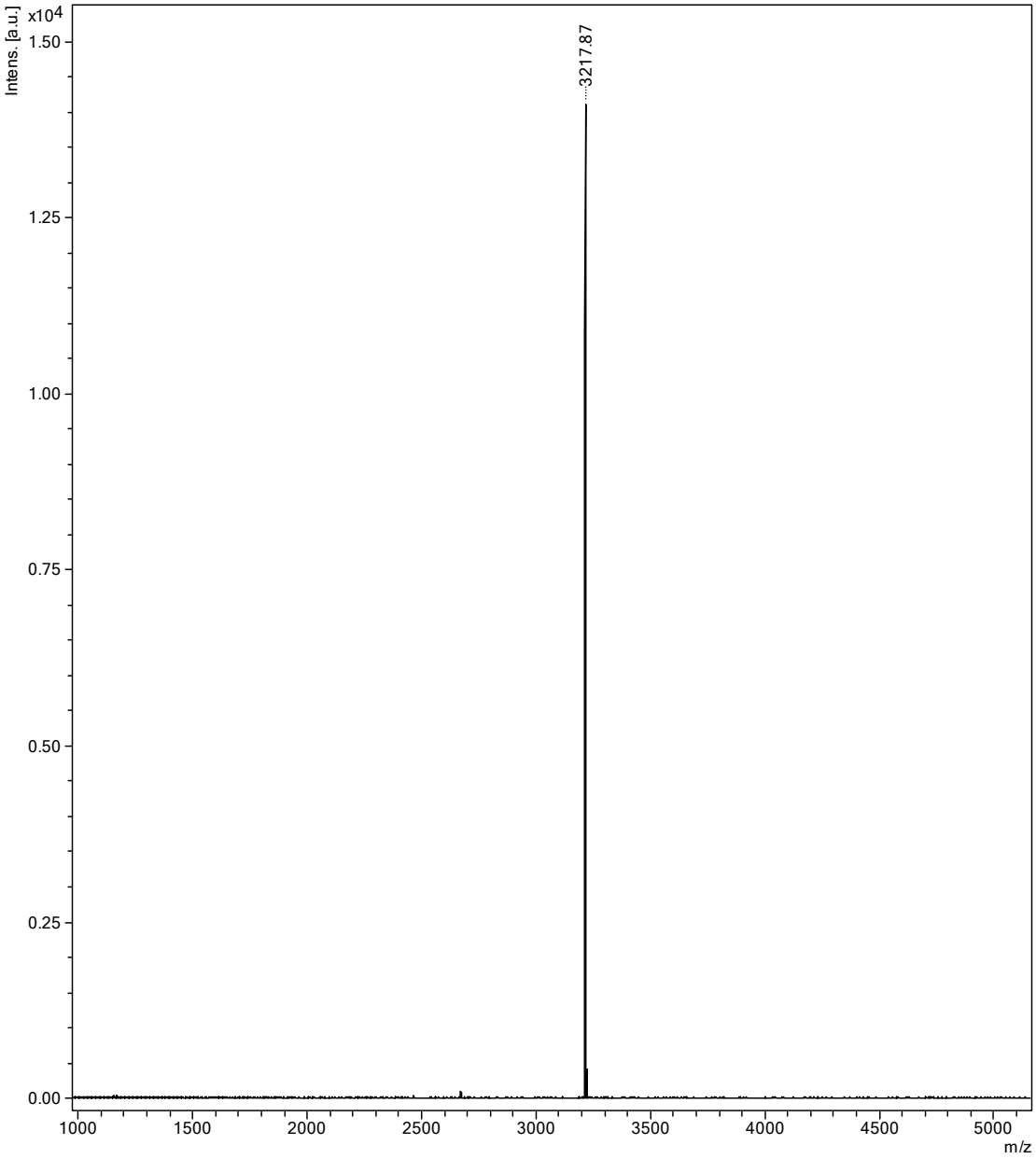


**Figure S14.** MS of compound 3-2.

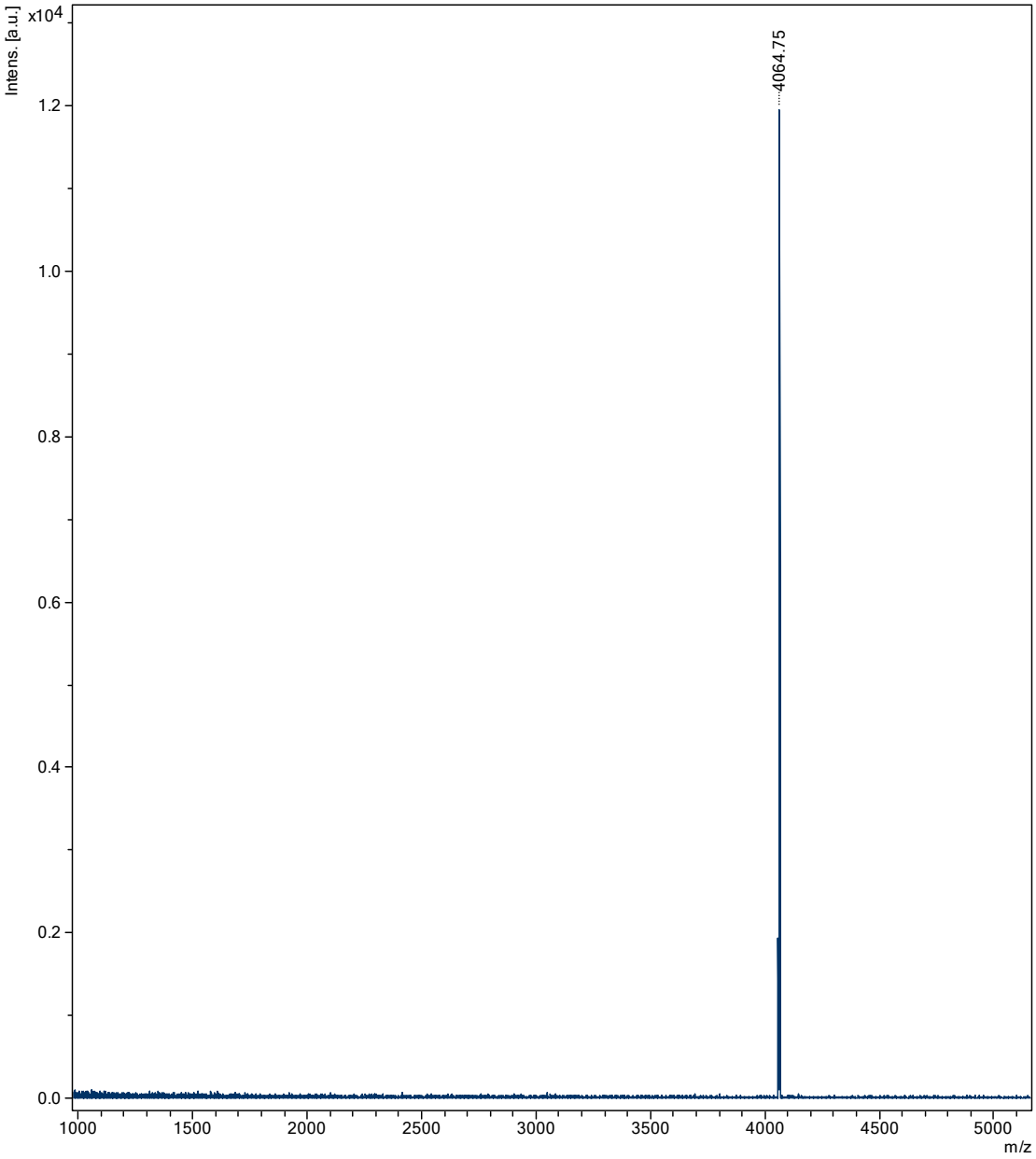


**Figure S15.** MS of CH8-8.

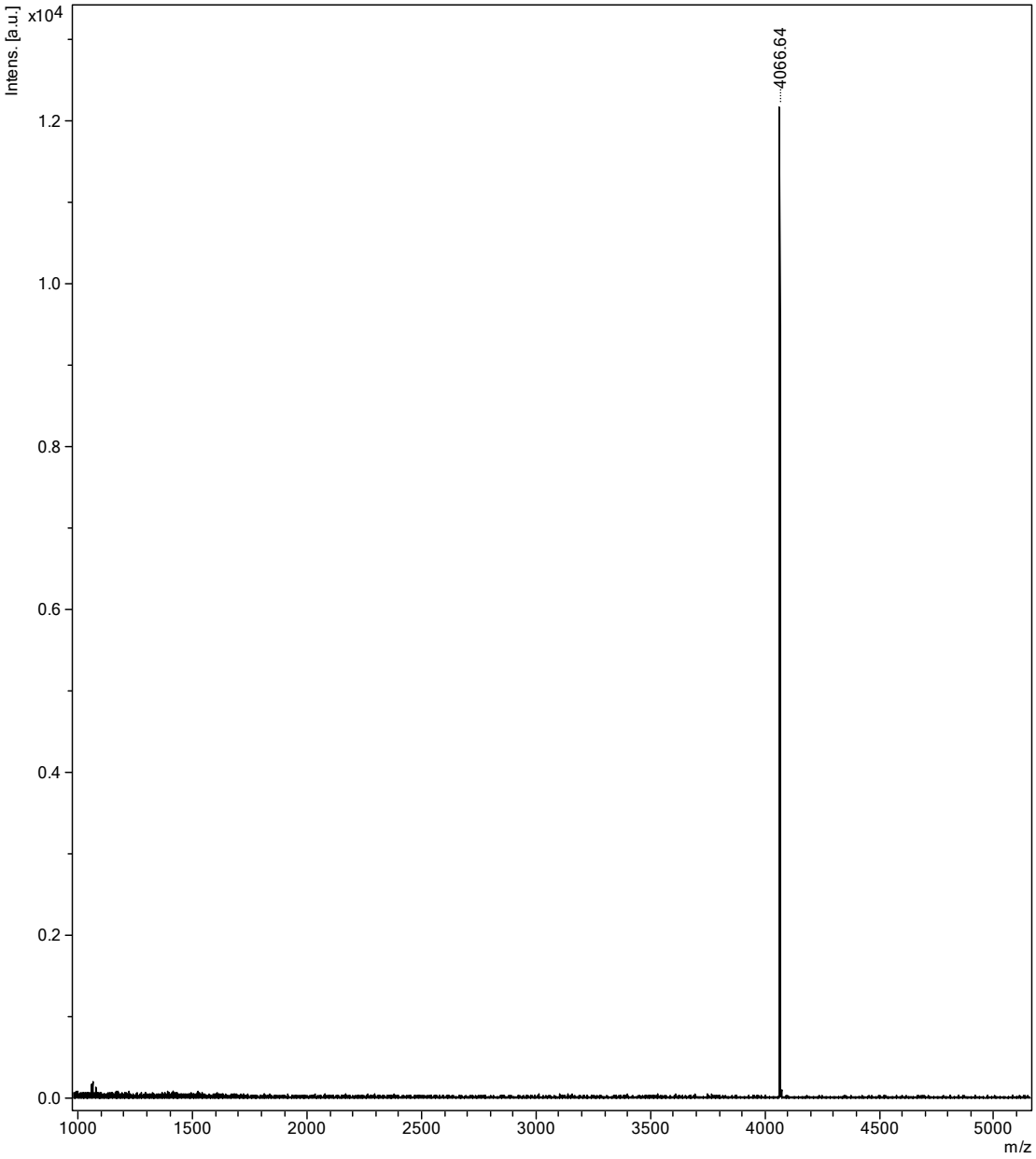


**Figure S16.** MS of CH8-9.

## 5. References.


1 H. Chen, Z. Zhang, P. Wang, Y. Zhang, K. Ma, Y. Lin, T. Duan, T. He, Z. Ma, G. Long, C. Li, B. Kan, Z. Yao, X. Wan and Y. Chen, *Energy & Environmental Science*, 2023, **16**, 1773-1782.

2 M. J. Frisch, G. W. Trucks, H. B. Schlegel, G. E. Scuseria, M. A. Robb, J. R. Cheeseman, G. Scalmani, V. Barone, G. A. Petersson, H. Nakatsuji, X. Li, M. Caricato, A. V. Marenich, J. Bloino, B. G. Janesko, R. Gomperts, B. Mennucci, H. P. Hratchian, J. V. Ortiz, A. F. Izmaylov, J. L. Sonnenberg, Williams, F. Ding, F. Lipparini, F. Egidi, J. Goings, B. Peng, A. Petrone, T. Henderson, D. Ranasinghe, V. G. Zakrzewski, J. Gao, N. Rega, G. Zheng, W. Liang, M. Hada, M. Ehara, K. Toyota, R. Fukuda, J. Hasegawa, M. Ishida, T. Nakajima, Y. Honda, O. Kitao, H. Nakai, T. Vreven, K. Throssell, J. A. Montgomery Jr., J. E. Peralta, F. Ogliaro, M. J. Bearpark, J. J. Heyd, E. N. Brothers, K. N. Kudin, V. N. Staroverov, T. A. Keith, R. Kobayashi, J. Normand, K. Raghavachari, A. P. Rendell, J. C. Burant, S. S. Iyengar, J. Tomasi, M. Cossi, J. M. Millam, M. Klene, C. Adamo, R. Cammi, J. W. Ochterski, R. L. Martin, K. Morokuma, O. Farkas, J. B. Foresman and D. J. Fox, *Journal*, 2016.

3 A. D. Becke, *The Journal of Chemical Physics*, 1993, **98**, 5648-5652.

4 P. J. Hay and W. R. Wadt, *The Journal of Chemical Physics*, 1985, **82**, 299-310.

5 R. Krishnan, J. S. Binkley, R. Seeger and J. A. Pople, *The Journal of Chemical Physics*, 1980, **72**, 650-654.